Synergy of surface textures on a hydraulic cylinder piston

Ying Zhang, Liangcai Zeng ✉, *Zhenpeng Wu, Xianzhong Ding, Kuisheng Chen*

Hubei Key Laboratory of Mechanical Transmission and Manufacturing Engineering, Wuhan University of Science and Technology, Wuhan, Hubei 430081, People's Republic of China
✉ *E-mail: 13277047582@163.com*

Published in Micro & Nano Letters; Received on 5th September 2018; Revised on 30th November 2018; Accepted on 20th December 2018

This paper explores the synergy mechanisms that are associated with the coexistence of multiple textures, to improve the precision control of a hydraulic servo cylinder. Based on the classical Reynolds equation, it establishes a single-texture and a nine-texture model to compare and study the synergy of surface textures. The film thickness is obtained under different working conditions for 1 N. Based on this parameter, it compares the simulation results from the two models with the experimental results to determine if the friction coefficient is reduced when multiple textures exist. When multiple textures exist, the inlet pressures of the central texture increase, but the peak pressure and cavitation pressure decrease. The synergy of the textures acts as an 'average pressure' and causes the pressure to decrease, which directly decreases the shear force. As the area ratio of the texture increases, the beneficial effect from the synergy gradually increases and then decreases, which implies that there is an optimum area ratio. The depth of the texture was 10 μm and the optimum depth-to-diameter ratio was 0.009. When the speed increases for a light load, the oil film thickness increases. However, this phenomenon does not substantially change the synergistic effect.

1. Introduction: When studying fluid lubrication, most scholars choose a single flow field for modelling and simulation. Geometric shape effects [1–3] and asymmetric surface textures [4] are studied via single-texture models. Mao and Zeng established an analytical mathematical model to describe a uniformly distributed microtexture cavitation [5]. Some relevant research on lateral traction in a laminar state has been previously studied [6]. However, the studies have shown that there are interactions between textures [7], and the combined lubrication effectiveness enhances lubricant flow from high- to low-pressure areas, which decreases the peak film pressure, increases the instantaneous film thickness and enhances the film bearing capacity. Thus, simulations that use a single-texture model have diminished accuracy.

Texture morphology has been studied in hydraulic cylinders [8, 9]. As an example, the grooves on the inner wall of a cylinder can effectively reduce wear [10–14]. In servo cylinders with gap sealing, microtexture surfaces can effectively improve the lubrication performance of piston–cylinder friction pairs [15–17]. Scholars have studied the tribological properties of textured hydraulic cylinders based on a single-texture model [18–20]. Therefore, to improve the control accuracy of servo cylinders, further in-depth research on the effects of microtexture dynamic pressure lubrication is necessary.

As a result, establishing a comparison between the two models and analysing the mechanism of action among the textures is beneficial to understand the mechanisms behind the texture in a gap-sealing hydraulic cylinder.

2. Theory: The microtextures are evenly engraved on the surface of a piston throughout the system, as shown in Fig. 1*a*. The specific distribution of textures on the piston is shown in Fig. 1*b* [7]. It is worth noting that the influence of the radius of curvature can be neglected, and the surface of the piston can be treated as a plane since the thickness of the interstitial oil film and the radial dimensions of the microtextures are small relative to the size of the piston [21].

The two different models for a textured surface are shown in Fig. 2. Fig. 2*a* shows a single-texture flow field model, which is presently the most commonly used version. Fig. 2*b* shows a nine-texture flow field model for studying the synergistic effects among different textures. We used the finite difference method and the over-relaxation iterative method to numerically solve the equation.

Using the classic Reynolds equation, we can compare the parameter differences and pressure distributions between the two models. To simplify the model and ensure that the magnitude of such a change can be neglected, the texture height is set to be much smaller than the diameter [22]. The parameter symbols and their meanings are shown in Table 1.

The classical Reynolds equation is shown in the equation below:

$$\frac{\partial}{\partial x}\left(\rho(h+\varepsilon)^3\frac{\partial p}{\partial x}\right)+\frac{\partial}{\partial y}\left(\rho(h+\varepsilon)^3\frac{\partial p}{\partial y}\right)=6\eta\frac{\partial}{\partial x}(u\rho(h+\varepsilon)) \quad (1)$$

Note that the following dimensionless parameters can be used to transform (1):

$$X=\frac{x}{L},\quad Y=\frac{y}{L},\quad H=\frac{h}{h_0}+\frac{\varepsilon}{h_0},\quad P=\frac{\mathrm{Ph}_0^2}{6uL\eta}$$

The dimensionless Reynolds equation is shown in the equation below:

$$\frac{\partial}{\partial X}\left(H^3\frac{\partial P}{\partial X}\right)+\frac{\partial}{\partial Y}\left(H^3\frac{\partial P}{\partial Y}\right)=\frac{\partial H}{\partial X} \quad (2)$$

After obtaining the pressure distribution, it is integrated over the entire control unit. Then, the dimensionless bearing capacity of the lubricating oil film can be obtained. The process of integration is shown in the equation below:

$$W=\int_0^1\int_0^1 P\,\mathrm{d}X\,\mathrm{d}Y \quad (3)$$

Considering that the surface of the piston is only affected by the oil film pressure, the frictional force of the lubricating oil film

doi: 10.1049/mnl.2018.5535

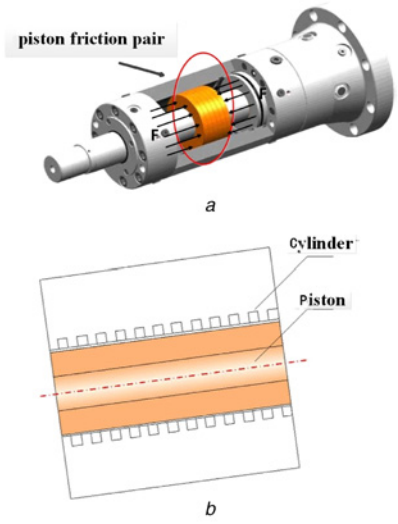

Fig. 1 *Gap-sealing hydraulic cylinder schematic diagram (authorised)*
a Textured cylinder liner–piston system
b Section view of the cylinder liner and piston

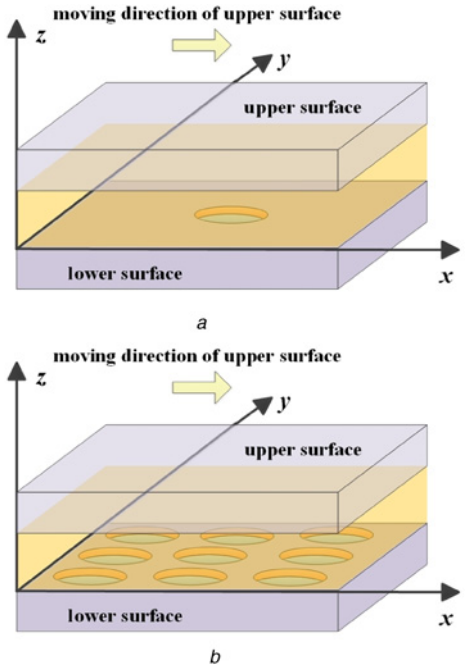

Fig. 2 *Two different models for a textured surface*
a Texture distribution in the single-texture model
b Texture distribution in the nine-texture model

can be obtained by integrating the shear stress in the fluid layer along the entire control unit, as shown in the equation below:

$$\mathrm{fh} = \int_0^1 \int_0^1 \left(\frac{H}{2} \frac{\partial P}{\partial X} + \frac{u\eta}{H} \right) \mathrm{d}X \, \mathrm{d}Y \tag{4}$$

By dividing the friction force by the bearing capacity, the friction factor for the piston surface can be obtained as shown in the equation below:

$$\mu = \frac{\mathrm{fh}}{W} \tag{5}$$

We define the area ratio of a single-textured area to be a unit Sp, which is defined as Sp = (texture area)/(L×L), as shown in Fig. 3.

According to the experimental setup, the load was set to 1 N. Therefore, by using the solution of the Reynolds equation, the thickness of the bearing oil film and the coefficient of friction can be obtained for various working conditions, as shown in Tables 2 and 3.

3. Experiment: An UMT-3 friction testing machine (UMT-3, Bruker, USA) is used for all experiments at room temperature. The specimens are smooth discs and copper rods with micro-textured topographies, as shown in Fig. 4.

Table 1 Symbols and parameters

Symbols	Parameter
h	oil film thickness without considering the experiment
$\boldsymbol{\varepsilon}$	additional film thickness caused by the presence of dynamic pressure during the experiment as shown in Table 1
u	velocity of the fluid
$\boldsymbol{\eta}$	dynamic viscosity of the oil, which is 0.1 Pa s
p	real pressure
$\boldsymbol{\rho}$	density of the oil, which is 0.875 kg/l
L	length of a square simulation unit (for the single-texture and nine-texture models, this length is 1.5 and 4.5 mm, respectively)
$\boldsymbol{h}_0$	gap between the piston and the cylinder liner (set to 10 μm)
P	dimensionless pressure
W	dimensionless bearing capacity of the lubricating oil film
fh	frictional force of the lubricating oil film
μ	friction factor

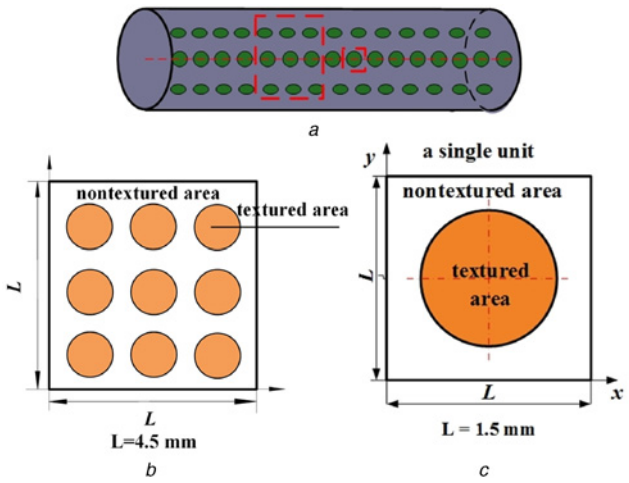

Fig. 3 *Model of the microtexture and geometry*
a Textured piston surface schematic
b Single-texture unit
c Nine-texture unit

Table 2 Bearing film thickness (μm) under different conditions

Sp	v, m/s						
	0.1	0.2	0.3	0.4	0.5	0.6	0.7
0.2288	15	19	19	19	21	21	24
0.3432	16	19	22	23	23	25	22
0.4576	16	21	22	22	24	25	26
0.5720	15	18	21	26	26	25	26

Table 3 Coefficient of friction under different conditions

Sp	*v*			
	0.2288 m/s	0.3432 m/s	0.4576 m/s	0.5720 m/s
0.1	0.0643	0.0885	0.1188	0.1645
0.2	0.0746	0.1149	0.1296	0.2143
0.3	0.0997	0.1162	0.1577	0.2174
0.4	0.1178	0.1247	0.1852	0.1673
0.5	0.1040	0.1339	0.1668	0.1788
0.6	0.1027	0.1103	0.1504	0.1904
0.7	0.0669	0.1258	0.1708	0.1526

Fig. 4*a* shows the UMT-3 friction tester and Fig. 4*b* shows the installation of the copper rods and disc. The end of the copper rod is textured and the disc below is smooth. Fig. 4*c* shows the texture distribution at the bottom of the copper rods. The disc diameter is 50 mm, the rod diameter is 6.3 mm, and the nine pockets are evenly distributed. Different copper rods have texture diameters of 540–1420 μm and the depth is 10 μm. The texture of a single copper rod is homogeneous. The copper rod makes a circular motion along the edge of the disc.

Mobil CI4 lubricant was chosen for this experiment, and its specific parameters are shown in Table 4. The lower end of the copper rod is completely immersed in the oil to ensure an oil-rich state.

The alignment is adjusted and the fixing screw above the copper rod is tightened and performed to ensure that the copper rod does not vibrate. The load is then set to 1 N and the associated speed is set as desired for different situations. The experiment is started

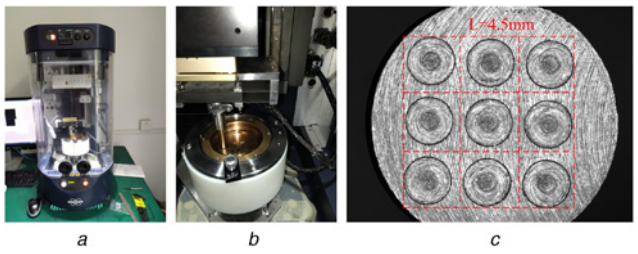

Fig. 4. *UMT-3 friction testing machine and the textured surface*
a The UMT-3 friction testing machine
b Assembly of test pieces
c The distribution of textures

Table 4 Mobil CI4 lubricant properties

Parameter	Value
density at 15°C, kg/l	0.8747
dynamic viscosity at −20°C, mPa s	5418
kinematic viscosity at 100°C, mm^2/s	14.4

Table 5 Coefficient of friction for different areas of ratios and speeds

Sp	*v*			
	0.2288 m/s	0.3432 m/s	0.4576 m/s	0.5720 m/s
0.1	0.0658	0.0914	0.1294	0.1795
0.2	0.0705	0.1117	0.1112	0.2136
0.3	0.1059	0.1164	0.1429	0.2000
0.4	0.0900	0.1174	0.1655	0.1302
0.5	0.1194	0.1276	0.1440	0.1455
0.6	0.1086	0.0987	0.1392	0.1780
0.7	0.0609	0.1298	0.0953	0.1300

Table 6 Results from the two models

	μ	*w*, N	Fh, N
single-texture texture model	0.1206	0.1118	0.0135
nine-texture texture model	0.1021	1.0055	0.1026
experimental result	0.1164	1.0387	0.1203

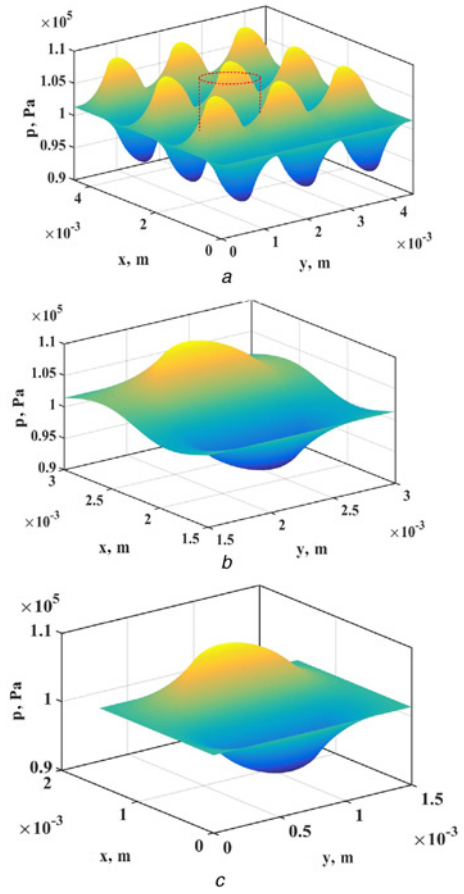

Fig. 5 *Comparison of the centre texture boundary conditions in the two models*
a Pressure distribution in the nine-texture model
b Centre texture pressure distribution in the nine-texture model
c Pressure distribution in the single-texture model

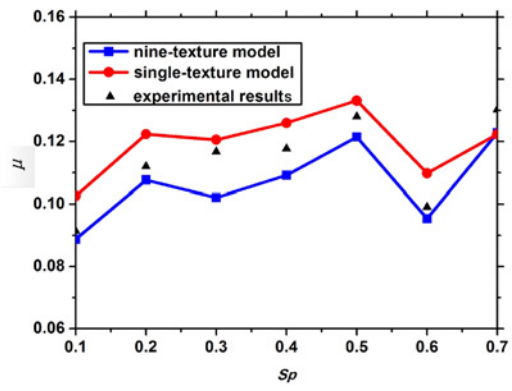

Fig. 6 *Friction coefficient results for the two models*

doi: 10.1049/mnl.2018.5535

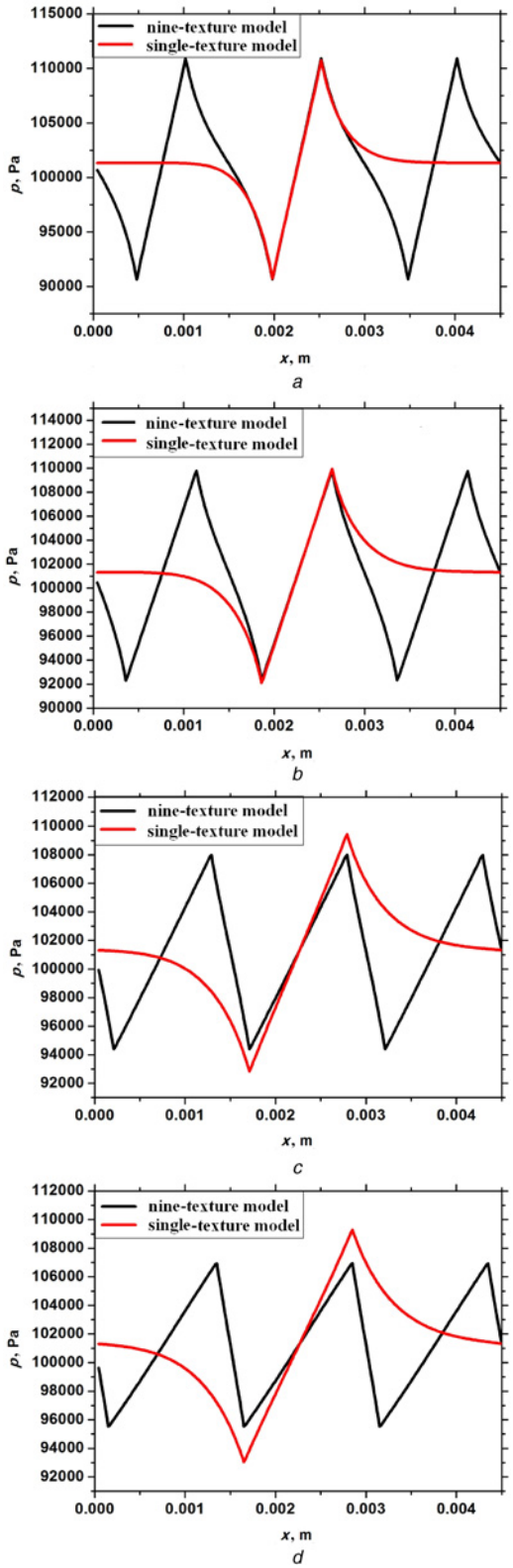

Fig. 7 *Comparison of the pressure distribution curves from the central texture section of the two models*
a Central texture cross-section pressure distribution curve when Sp = 0.1
b Central texture cross-section pressure distribution curve when Sp = 0.2
c Central texture cross-section pressure distribution curve when Sp = 0.4
d Central texture cross-section pressure distribution curve when Sp = 0.5

by lowering the copper rod toward the disc by ~5 mm. During the experiment, the rod automatically drops to the appropriate film thickness. Prior to each test, the machine was run for 30 min to ensure operational stability. Each experimental set lasts 5 min and is repeated three times to ensure its accuracy and repeatability. During the circular motion of the copper rod, the upper sensor measures the value of the shear force and the friction coefficient is determined. From the results, the friction coefficients under different working conditions can be obtained as shown in Table 5.

In theory, the single-hole and nine-hole texture models, as well as the experimental results, should be completely consistent. However, in practise, there are differences between the results; these differences are analysed in detail in the following sections.

4. Results and discussion

4.1. Synergistic effect of the nine-texture texture model: MATLAB was used to simulate a case, where Sp = 0.3 and $v = 0.3432$ m/s. Table 6 shows the value of $\boldsymbol{\mu}$, $\boldsymbol{w}$, and **Fh** for the two models.

The parameter values in the single-texture model must be multiplied by nine to compare with the parameter values in the nine-texture model. When the same load is applied to both models, the shear performance of the nine-texture model is smaller than the single-texture model, which directly leads to a reduction in the friction coefficient. The shear force is determined by the rate of change in the pressure. The only difference between the two models is the number of textures. Therefore, there is a mutual influence between pluralities of textures.

To further analyse this impact, we compare the pressure distribution clouds from the two models as shown in Fig. 5.

From Figs. 5*b* and *c*, we see that the surrounding textures increase the inlet of the central texture in the nine-texture model, and the added value is ~1500 Pa.

Therefore, when there are multiple textures, the central texture is affected by the others, which causes the boundary pressure to increase. This increase in boundary pressure results in a decrease in the shear force and provides better lubrication, which thereby acts as a synergistic effect.

4.2. Synergy of the different sizes of the textures: In this section, the synergistic effects of different texture radii are studied. Fig. 6 shows a comparison of the friction coefficients from the two models when $v = 0.3432$ m/s.

The simulation results for the two models are similar to the experimental results, but it is obvious that the lubrication for the friction pair surface is better when multiple textures coexist. Simultaneously, as the area ratio increases, the distance between the two lines first increases and then decreases. In other words, the positive influence of the synergistic effect first increases and

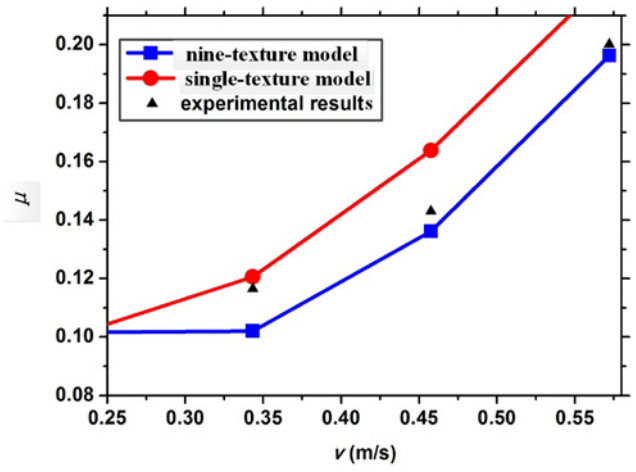

Fig. 8 *Friction coefficient variation as a function of velocity for the two models*

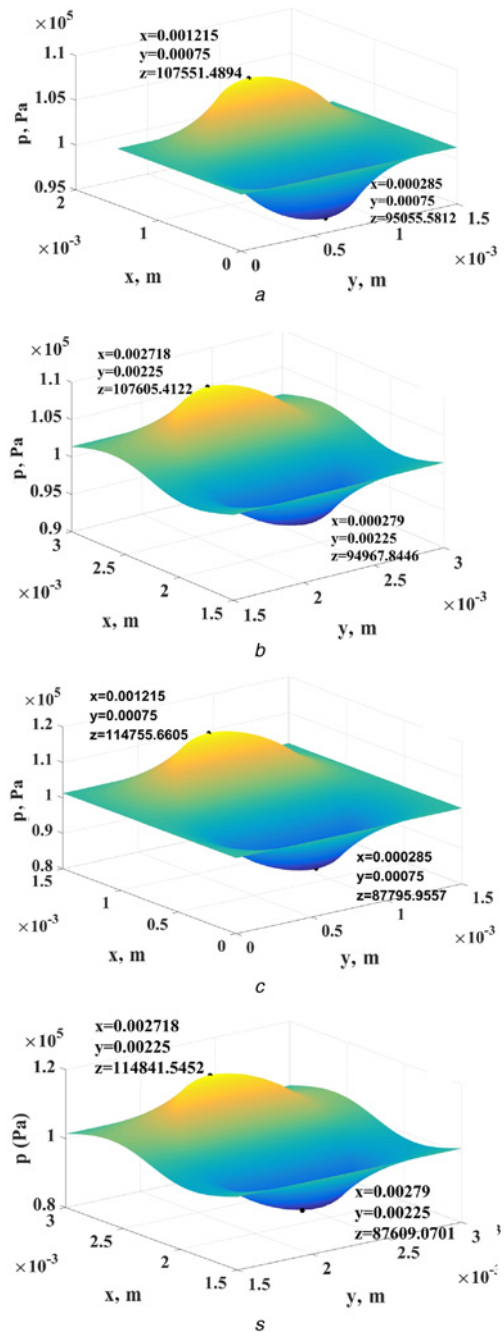

Fig. 9 *Pressure distributions for the two models at different speeds*
a Pressure distribution of the single-texture model at $v = 0.2288$ m/s
b Pressure distribution of the nine-texture model at $v = 0.2288$ m/s
c Pressure distribution of the single-texture model at $v = 0.5720$ m/s
d Pressure distribution of the nine-texture model at $v = 0.5720$ m/s

then decreases. When Sp = 0.4, synergy has the best effect on the lubrication performance and the optimum area ratio is 0.009.

Fig. 7 shows a comparison of the pressure distribution curves from the central texture section of the two models. The peak pressure of the central texture is 'swallowed' by the latter texture, but the cavitation area is 'supplemented' by the previous texture.

The positive vertical separation of the black line above the red line represents a positive synergistic effect and vice versa. Larger texture areas correspond to more obvious 'average effects' of the synergy. As the area ratio increases, the positive effect gradually decreases, and the negative effect gradually increases. Therefore, there is an optimum area ratio when the two effects reach equilibrium, which is one of the reasons for implementing the optimal aspect ratio.

4.3. Effect of velocity on the synergy: In this section, the effect of different velocities on the synergy of the textures is studied. To examine this, the velocities are set as 0.2288, 0.3432, 0.4576, and 0.5702 m/s, and the area ratio is set to 0.3. The resulting friction coefficients are shown in Fig. 8.

Table 1 shows that for the same light load, the thickness of the oil film increases. As the speed increases, the friction coefficients from both models increase; however, the rate of the increase is essentially the same in both models, which indicates that the synergy exists, but does not change with increasing speed.

Under different speed conditions, the dynamic pressure profiles for the two models (the single-texture model and the central texture of the nine-texture model) are compared.

The synergistic effect simultaneously acts on the peak and cavitation regions. The increase in speed leads to an increase in dynamic pressure (increase of 7200 Pa in the peak area), but there is no significant change in the synergistic effect (just decrease of 45–90 Pa in the peak area), as the results from the two models are not very different (Fig. 9).

5. Conclusions: A single-texture model and a nine-texture model were established and compared in this work. After analysis, we determined that synergy between the texture models exists between the texture models. In terms of the specific performance, as a result of the effect of the surrounding textures, the inlet and outlet pressures of the central texture increase, while the peak pressure and the cavitation decrease. The specific value added is related to the working environment. For example, the inlet pressure of the central texture is increased by 1500 Pa when Sp = 0.3 and $v = 0.3432$ m/s. Synergy mainly plays the role of an 'average pressure', which means that it decreases the rate of pressure change. Therefore, the shearing force from the entire textured surface is reduced, and the bearing capacity mostly remains unchanged, which results in a reduced friction coefficient. As a result, in the tribological analysis of a hydraulic servo cylinder, the influence of the synergistic effect should be taken into consideration.

We also considered the change in the friction coefficient in both two models with different area ratios and velocities. As the area ratio of the texture increases, a synergistic enhancement occurs between the texture models. The beneficial effect of the synergy first increases and then decreases as the area ratio of the texture increases. In this Letter, the texture depth is 10 μm, and the synergy effect on the lubrication effect is best when the depth-to-area ratio is 0.009. For a light load, the film thickness changes with speed, and the synergistic exists, but does not result in substantial change.

6. Acknowledgment: The project was supported in part by the National Natural Science Foundation of China under grants nos. 51475338, 51175386, and 51405350.

7 References

[1] Syed I., Sarangi M.: 'Hydrodynamic lubrication with deterministic microtextures considering fluid inertia effect', *Tribol. Int.*, 2014, **69**, (1), pp. 30–38
[2] Yu H., Wang X., Zhou F.: 'Geometric shape effects of surface texture on the generation of hydrodynamic pressure between conformal contacting surfaces', *Tribol. Lett.*, 2010, **37**, (2), pp. 123–130
[3] Sedlaček M., Podgornik B., Ramalho A., *ET AL.*: 'Influence of geometry and the sequence of surface texturing process on tribological properties', *Tribol. Int.*, 2017, **115**, pp. 268–273
[4] Schuh J.K., Ewoldt R.H.: 'Asymmetric surface textures decrease friction with Newtonian fluids in full film lubricated sliding contact', *Tribol. Int.*, 2016, **97**, (9), pp. 490–498

doi: 10.1049/mnl.2018.5535

[5] Mao Y., Zeng L.C., Lu Y.: 'Modeling and optimization of cavitation on a textured cylinder surface coupled with the wedge effect', *Tribol. Int.*, 2016, **104**, pp. 212–224
[6] Wu Z., Zeng L., Chen X., *ET AL.*: 'Lateral traction of laminar flow between sliding pair with heterogeneous slip/no-slip surface', *AIP Adv.*, 2017, **7**, pp. 115–208
[7] Yin B.F., Qian Y.Q., Wang B.W., *ET AL.*: 'Combined lubrication effectiveness of surface textures on diesel cylinder liner', *Trans. CSICE*, 2014, **32**, (2), pp. 178–185
[8] Rahmani R., Shirvani A., Shirvani S.: 'Optimised textured surfaces with application in piston-ring/cylinder liner contact', in Rahnejat H. (ED.): '*Tribology and Dynamics of Engine and Powertrain: Fundamentals, Applications and Future Trends*' (Woodhead Publishing, Cambridge, 2010, 14th edn.), pp. 470–517
[9] Pei S., Xu H., Yun M., *ET AL.*: 'Effects of surface texture on the lubrication performance of the floating ring bearing', *Tribol. Int.*, 2016, **102**, pp. 143–153
[10] Shi X., Ni T.: 'Effects of groove textures on fully lubricated sliding with cavitation', *Tribol. Int.*, 2011, **44**, (12), pp. 2022–2028
[11] Mezghani S., Demirci I., Zahouani H., *ET AL.*: 'The effect of groove texture patterns on piston-ring pack friction', *Prec. Eng.*, 2012, **36**, (2), pp. 210–217
[12] Grabon W., Pawlus P., Wos S., *ET AL.*: 'Effects of honed cylinder liner surface texture on tribological properties of piston ring–liner assembly in short time tests', *Tribol. Int.*, 2017, **113**, pp. 137–148
[13] Yu G., Zeng L., Mao Y., *ET AL.*: 'Numerical analysis of the friction property of microgroove texture on the piston surface of hydraulic cylinder', *J. Wuhan Univ. Sci. Technol.*, 2015, **3806**, pp. 436–439
[14] Chang Q.Y., Zheng X.L., Liu Q.: 'Numerical simulation on the lubrication performance of surface textured piston rings', *Adv. Mater. Res.*, 2010, **199-200**, pp. 734–738
[15] Yu G., Zeng L., Mao Y., *ET AL.*: 'Analysis on hydrodynamic lubrication performance of microtexture on hydraulic cylinder piston surface', *Mech. Sci. Technol. Aerosp. Eng.*, 2017, **3612**, pp. 1823–1829
[16] Vlădescu S.C., Medina S., Olver A.V., *ET AL.*: 'Lubricant film thickness and friction force measurements in a laser surface textured reciprocating line contact simulating the piston ring–liner pairing', *Tribol. Int.*, 2016, **98**, pp. 317–329
[17] Hu Y.: 'Effects of different surface textures on friction and wear performance of diesel cylinder liner–piston ring', *Lubr. Eng.*, 2013, **38**, (4), pp. 57–62
[18] Yu H., Wang X., Yuan S., *ET AL.*: 'Theoretical analysis on hydrodynamic lubrication of cylinder micro-dimple surface texture', *J. Nanjing Univ. Aeronaut. Astronaut.*, 2010, **42**, (2), pp. 209–213
[19] Yousfi M., Mezghani S., Demirci I., *ET AL.*: 'Tribological performances of elliptic and circular texture patterns produced by innovative honing process', *Tribol. Int.*, 2016, **100**, pp. 255–262
[20] Usman A., Park C.W.: 'Numerical investigation of tribological performance in mixed lubrication of textured piston ring–liner conjunction with a non-circular cylinder bore', *Tribol. Int.*, 2017, **105**, pp. 148–157
[21] Fu Y.H., Zhang H.W., Ji J.H., *ET AL.*: 'Numerical analysis on the lubrication performance of piston ring by surface micro-texturing', *Trans. CSICE*, 2009, **27**, (2), pp. 180–185
[22] Mall A., Agrawal A., Singh R.K., *ET AL.*: 'Numerical characterization of laminar bulk flow over textured surfaces', *J. Micro/Nanolithogr. Mems Moems*, 2011, **10**, (2), p. 023008